

Article

Resonance Characteristics of the LLC Resonant Half-Bridge Converter for the Rapid Charging of Personal Mobility Device Smart Batteries

Jin-Yong Bae

Department of Electric Vehicle Engineering, Dongshin University, Naju 58245, Republic of Korea; bji@dshu.ac.kr; Tel.: +82-61-330-7652

Abstract: This study discusses the resonance characteristics of the LLC resonant half-bridge converter and smart battery charging for the fast charging of personal mobility devices (e.g., electric kickboards, segways, hoverboards, electric bicycles, and electric motorcycles), whose use is rapidly increasing. Through the analysis of resonance characteristics, this study aims to validate that $f_s > f_0$ is the most appropriate correlation in the relationship between resonant frequency (f_0) and switching frequency (f_s) that is suitable for the rapid charging of batteries of personal mobility devices. Additionally, the proposed half-bridge converter does not charge the battery from discharge or misconnection based on the detection of the battery voltage for the batteries of personal mobility devices. Therefore, the proposed converter suggests a charging system based on battery state detection that stably performs rapid charging of the batteries of personal mobility devices by equalizing the battery voltage and the charger voltage through a pre-charge operation.

Keywords: personal mobility devices; rapid charging; smart battery charging; LLC; half-bridge; converter



Citation: Bae, J.-Y. Resonance Characteristics of the LLC Resonant Half-Bridge Converter for the Rapid Charging of Personal Mobility Device Smart Batteries. *Energies* **2023**, *16*, 6538. <https://doi.org/10.3390/en16186538>

Academic Editors: Giuseppe Buja, Guidong Zhang, Gong Zheng, Xiangke Li, Minghao Wang, Shuo Yan and Qingsong Wang

Received: 26 July 2023

Revised: 2 September 2023

Accepted: 7 September 2023

Published: 11 September 2023



Copyright: © 2023 by the author. Licensee MDPI, Basel, Switzerland. This article is an open access article distributed under the terms and conditions of the Creative Commons Attribution (CC BY) license (<https://creativecommons.org/licenses/by/4.0/>).

1. Introduction

This study discusses the resonance characteristics of the LLC resonant half-bridge converter for the fast charging of batteries of personal mobility devices and smart battery charging. Recently, a new type of transportation that can accomplish tens of kilometers of travel using an AC 220 V battery has been realized.

Particularly, the new means of transportation, including electric wheelchairs, electric bicycles, electric motorcycles, electric wheels, hoverboards, segways, and micro electric vehicles, basically does not generate pollution or fine dust, such as carbon (CO₂) and nitrogen (NO_x). As well as this advantage, it is based on a simple payment method using a smart phone and a location-based global positioning system [1,2].

Lee et al. analyzed and compared an asymmetric half-bridge (AHB) converter, a two-transistor forward converter, and an active clamp forward converter. They determined that among the three topologies, the AHB converter with the smallest current flowing through the switch, diode, and inductor of the converter is the most efficient [3].

Yong et al. analyzed and compared the topologies of an AHB converter and an LLC resonant converter in terms of the conduction and switching loss of the primary side of the transformer. They found that the efficiency of the LLC resonant converter is about 2~3% higher than that of the AHB converter [4].

Lu et al. [5] and Choi [6] analyzed the series resonance characteristics of LLC resonant converters, and Beiranvand et al. investigated the optimal design method of LC-LLC resonant converters that are suitable for large output voltage and load fluctuations [7].

Gu et al. studied an LLC series resonant converter based on a three-level topology suitable for high voltage input and high power output [8]. Yong et al. proposed a magnetic-type LLC resonant converter [9].

Kim et al. proposed LLC resonance on the secondary side of a transformer for the transformation of various resonance methods in relation to the LLC resonance type [10].

Chen et al. employed LLC resonance in a bidirectional converter [11], Cheng et al. analyzed the LLC parallel resonance method [12], and Cheng et al. analyzed the LLCC parallel resonance method [13].

Recently, studies on the topology suitable for high current loads have been actively conducted. Feng et al. determined that the on-resistance (R_{ds_on}) of the switch is smaller than the voltage drop (V_D) of the rectifier diode on the secondary side of the transformer, resulting in a low voltage and high current output. Additionally, they studied a suitable synchronous-rectifier-based LLC converter [14].

Lin et al. proposed an LLC converter based on a current doubler rectifier circuit [15], and Mishima et al. proposed a full-bridge-based converter with four switches for large power conversion [16]. Bhat et al. designed a bridge circuit with six switches [17].

Yi and Moon proposed a power supply wherein two LLC resonant converters operate in parallel and perform interleaved operations [18], and Gu et al. proposed a voltage doubler circuit that is suitable for the high voltage output of an LLC converter [19].

To reduce the switching loss of an LLC resonant converter, Mishima et al. proposed the zero current switching (ZCS) method based on the arrangement of an active clamp circuit, wherein an auxiliary switch and auxiliary diode are placed in parallel with the main switch [20]. Huang studied operating waveform for LLC resonant converter according to the resonant frequency [21], and Han et al. analyzed efficiency of the LLC resonant converter according to the resonant frequency [22].

Various studies related to LLC resonant converters are being conducted [23–27].

Through resonance characteristic analysis, this study aims to validate that $f_S > f_0$ is the most appropriate correlation in the relationship between resonant frequency (f_0) and switching frequency (f_S) that is suitable for the rapid charging for batteries of personal mobility devices.

The proposed smart battery charging system is technically characterized; in other words, no initial overcurrent occurs during battery charging and the battery does not charge when it is discharged or mis-wired according to the detection of the battery voltage. This study proposes a battery charging system based on battery state detection that stably performs the rapid charging of the batteries of personal mobility devices by equalizing the battery and charger voltages through a pre-charge operation.

Based on the 1.5 kW class prototype, the efficiency and suitability of the proposed converter for the rapid charging of the batteries of personal mobility devices are investigated, and the feasibility of the proposed converter is discussed through simulations and experiments.

2. Characterization of the Proposed LLC Resonant Half-Bridge Converter

Figure 1 displays the circuit diagram of the LLC resonant AHB converter. The proposed LLC resonant AHB converter circuit comprises main switches (S_1 and S_2), the resonant network (L_r , C_r , and L_m), a main transformer, and secondary rectifier diodes (D_1 and D_2). In the proposed converter, the switches and the secondary rectifier diodes operate at zero voltage switching (ZVS) and ZCS and $f_S > f_0$.

Since the proposed converter is based on the series resonance method, magnetizing inductance (L_m) participates in the resonance and the input/output voltage conversion ratio (M_g) can be derived based on f_0 .

Figure 2 displays the operating waveform of the LLC resonant AHB converter that is suitable for battery charging. For the mode analysis of the LLC resonant AHB converter, the following assumptions are made.

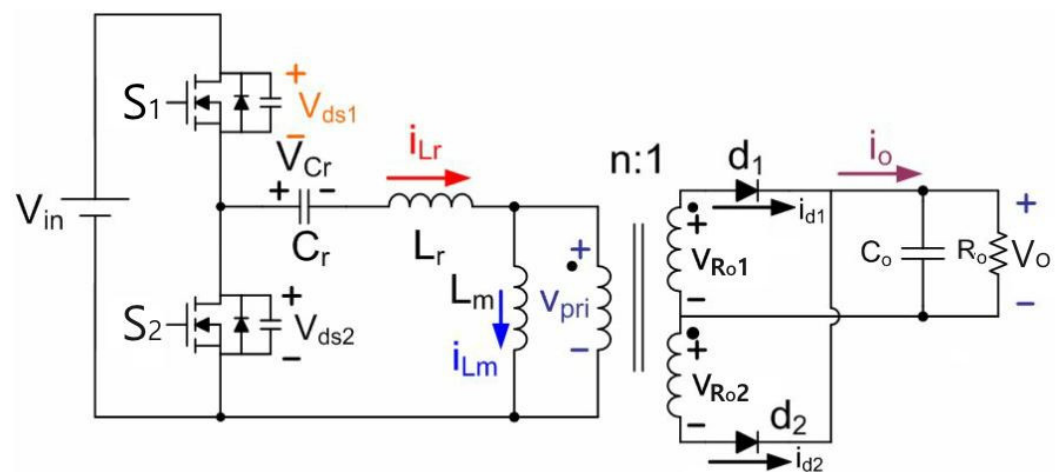


Figure 1. LLC Resonant AHB converter.

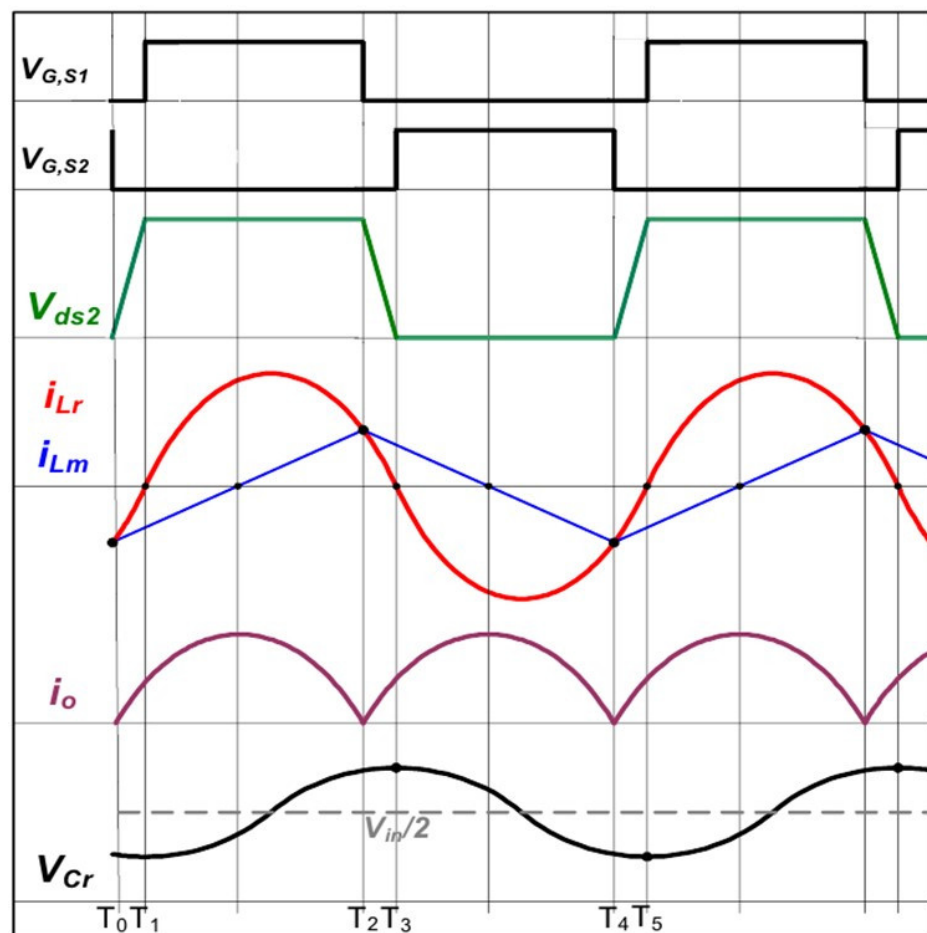


Figure 2. Operating waveform for proposed LLC resonant AHB converter.

First, the main switches and secondary rectifier diodes are ideal.

Second, the main switches comprise an ideal switch and an anti-parallel diode.

Third, the transformer considers the ideal L_m and leakage inductor (L_r).

Fourth, the output capacitor (C_o) is very large and operates as a constant voltage source in a steady state.

Fifth, the LLC resonant converter operates in a steady state.

(1) Mode 1 ($T_0 - T_1$)

Figure 3 shows the current conduction path of mode 1 and the current flow for the dead time area corresponding to the mode 1 ($T_0 - T_1$) section in Figure 2. The switch S_2 is on in the period before $t = T_0$. The switch S_2 is turned off at $t = T_0$. Here, the current flowing in L_r is negative ($-$) due to the continuous flow and the resonance path $L_m - L_r - C_r - S_1 - V_{in}$ results in the flow of a negative ($-$) L_r current.

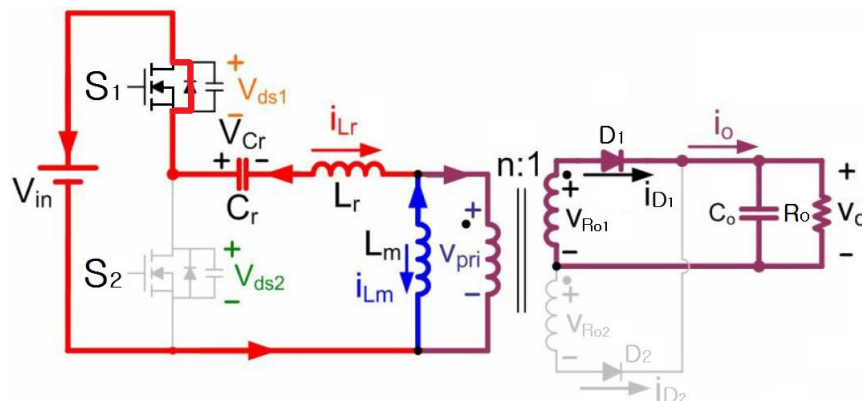


Figure 3. Current conduction path in mode 1.

Therefore, since the voltage across switch $S_1 = 0$, at $t = T_1$, the switch S_1 is turned on under the condition of ZVS; thus, the switching turn-on loss is zero (0).

The secondary rectifier diode D_1 of the transformer secondary side is conducting and the current continuously flows. The voltage across the transformer's L_m is $\frac{V_o}{n}$ (where n is the winding ratio of the transformer), and the current of the transformer's L_m increases with a slope of $\frac{V_o}{n} L_m$. Therefore, in mode 1, the current of L_r is relatively larger than the current of L_m .

(2) Mode 2 ($T_1 - T_2$)

Figure 4 shows the current conduction path of mode 2. It displays the current flow for the area corresponding to the mode 2 ($T_1 - T_2$) section in Figure 2. As shown in the mode 2 section waveform in Figure 2, at $t = T_1$, the switch S_1 is turned on under the condition of ZVS. Moreover, the current of L_r has a positive ($+$) value and gradually increases, and the voltage across both ends of L_m is applied as $\frac{V_o}{n}$. Thus, the current of the L_m of the transformer increases with a slope of $\frac{V_o}{n} L_m$. During the mode 2 section, $L_r - C_r$ resonance current flows and series current resonance is achieved. The rectifying diode D_1 on the secondary side of the transformer is conducting and the current continuously flows. The remaining half-cycle follows the same process as that of mode 1.

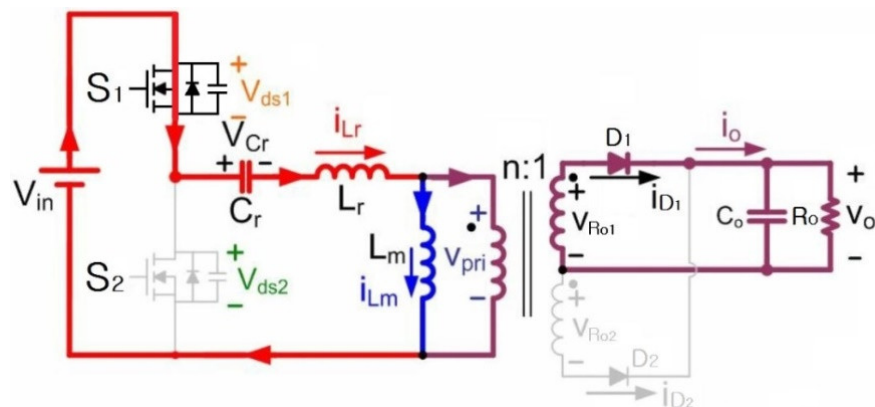


Figure 4. Current conduction path in mode 2.

Figure 5 shows the operating waveform of the LLC resonant converter according to the resonant frequency [21]. To date, various studies have been conducted on the design of the resonant frequency of the LLC resonant converter. For LEDs and laptops with relatively small load fluctuations, studies have been conducted to design the LLC resonant frequency as $f_s = f_0$ or $f_s < f_0$ [4–9].

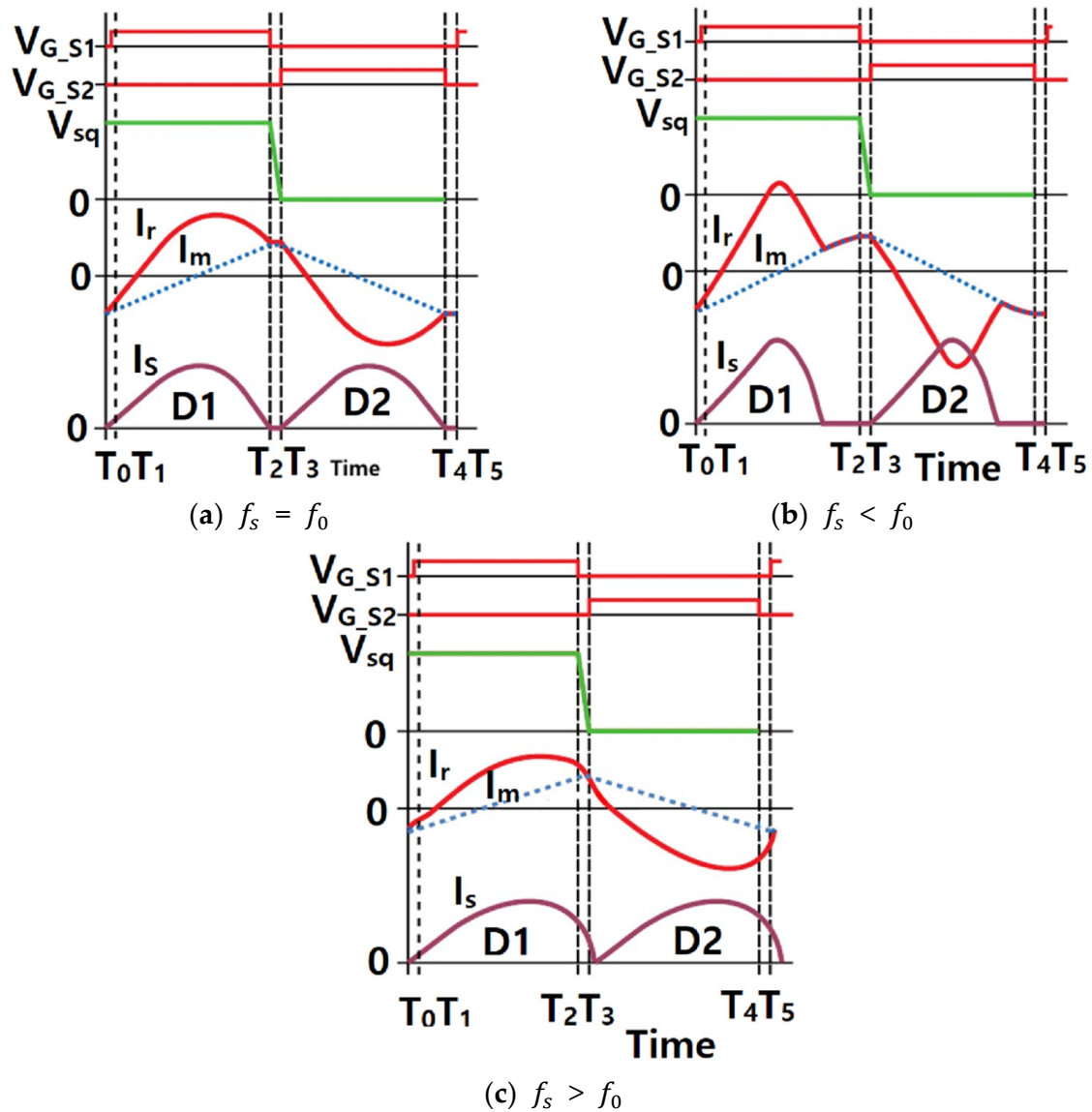


Figure 5. Operating waveform of the LLC resonant converter according to resonant frequency [21].

For LEDs and laptops, wherein the load characteristics are almost unchanged, the LLC resonant frequency setting is designed under the condition of $f_s = f_0$ or $f_s < f_0$ to ensure full or heavy load, respectively. It was proposed to supply the power necessary during the heavy load condition [4–9]. This method exhibits excellent efficiency under full and heavy load conditions, but it is not suitable for battery charging because the battery efficiency rapidly deteriorates under light load conditions [6,22].

Figure 6 shows the efficiency curves at resonant frequencies $f_s > f_0$ and $f_s \leq f_0$ [6,22]. As shown in Figure 6, the efficiency of the converter at the resonant frequency is about 90% under heavy load, but the efficiency rapidly decreases under light load. At the resonant frequency $f_s > f_0$, the efficiency curve continuously exhibits high efficiency under full and heavy load as well as light load conditions [6,22].

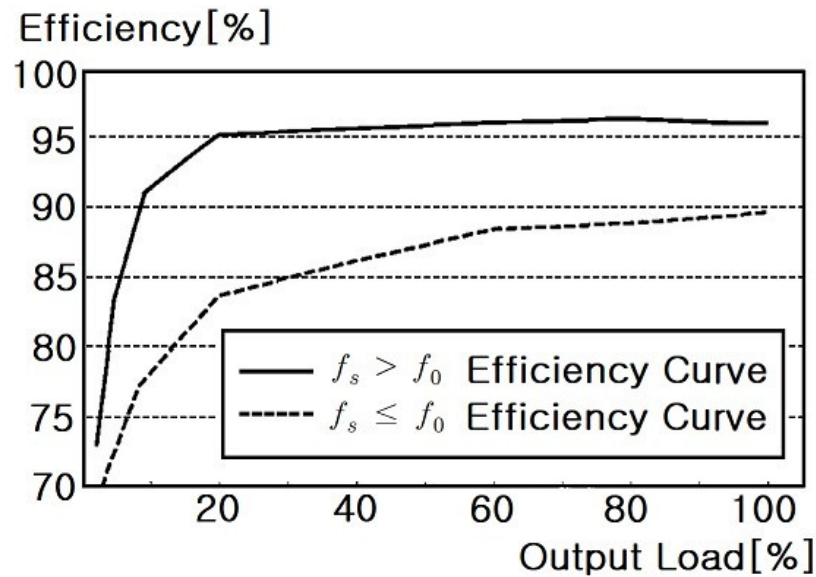


Figure 6. Efficiency curve at resonant frequency $f_s > f_0$ and $f_s \leq f_0$ [22].

As shown in Figure 6, the resonant frequency $f_s > f_0$ of the proposed AHB converter is more than 5% under the full load condition and more than 10% under the light load condition. Thus, compared to existing converters with $f_s \leq f_0$, the proposed converter exhibits higher efficiency [6,22].

Therefore, herein, the LLC resonant AHB converter is applied as the circuit implementation method of a rapid charging apparatus for charging the batteries of personal mobility devices. For battery charging, a full load or heavy load is applied initially and a light load is continuously applied at the end. The validity of the proposed method was verified via comparison with the results of previous studies [6,22].

3. Input/Output Voltage Conversion Ratio of LLC Resonant Converter

Figure 7 shows the LLC resonant AHB converter circuit and the AC equivalent circuit. From Figure 7, the following relational expressions (1) and (2) can be derived [6].

$$V_{R_o}^F = \frac{4V_o}{\pi} \sin(\omega t) \quad (1)$$

$$I_{ac} = \frac{\pi I_o}{2} \sin(\omega t) \quad (2)$$

Therefore, based on the output voltage conversion formula, the equivalent load resistance (R_{ac}) can be expressed as follows:

$$R_{ac} = \frac{V_{R_o}^F}{I_{ac}} = \frac{8}{\pi^2} \frac{V_o}{I_o} = \frac{8}{\pi^2} R_o \quad (3)$$

Considering the transformer turns the ration ($n = \frac{N_p}{N_s}$), the R_{ac} is obtained as

$$R_{ac} = \frac{8}{\pi^2} \left(\frac{N_p}{N_s} \right)^2 R_o = \frac{8}{\pi^2} n^2 R_o \quad (4)$$

From the AC equivalent circuit of the LLC resonant converter shown in Figure 8, the impedances of L_r , C_r , and L_m can be defined as follows.

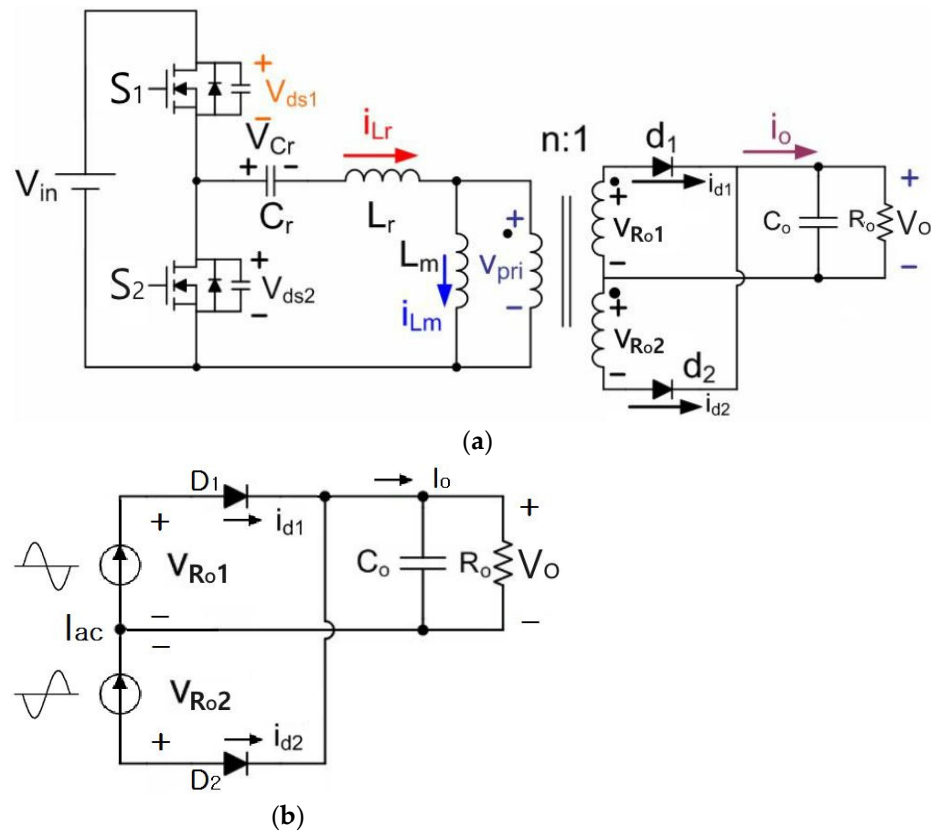


Figure 7. Derivation process of the equivalent load resistance (R_{ac}). (a) LLC resonant AHB converter. (b) Simplification for deriving the equivalent load resistance (R_{ac}).

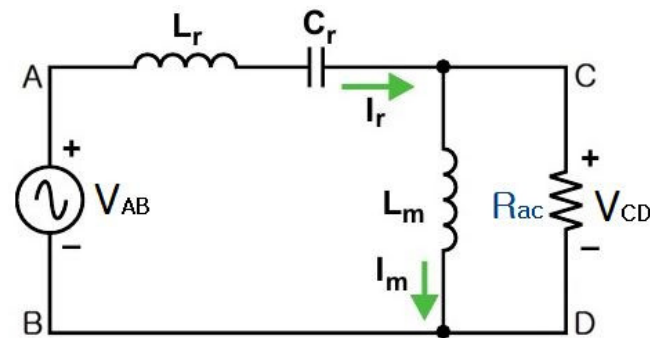


Figure 8. AC equivalent circuit of LLC resonant converter.

$$\text{Impedance of } L_r: X_{L_r} = \omega L_r$$

$$\text{Impedance of } C_r: X_{C_r} = \frac{1}{\omega C_r}$$

$$\text{Impedance of } L_m: X_m = \omega L_m$$

Based on the impedances defined above, the voltage ratio between the input (V_{AB}) and output (V_{CD}) of the LLC resonant converter (Figure 8) can be expressed as Equations (5)–(8).

$$\frac{V_{CD}}{V_{AB}} = \frac{jX_m R_{ac} / (jX_m + R_{ac})}{\frac{jX_m R_{ac}}{jX_m + R_{ac}} + jX_{L_r} - jX_{C_r}} \quad (5)$$

$$\frac{V_{CD}}{V_{AB}} = \frac{jX_m R_{ac}}{jX_m R_{ac} + (jX_{L_r} - jX_{C_r})(jX_m + R_{ac})} \quad (6)$$

$$\frac{V_{CD}}{V_{AB}} = \frac{1}{1 + j\frac{X_{L_r}}{R_{ac}} - j\frac{X_{C_r}}{R_{ac}} + \frac{X_{L_r}}{X_m} - \frac{X_{C_r}}{X_m}} \quad (7)$$

$$\frac{V_{CD}}{V_{AB}} = \frac{1}{\left(1 + \frac{X_{Lr} - X_{Cr}}{X_m}\right) + j\left(\frac{X_{Lr} - X_{Cr}}{R_{ac}}\right)} \quad (8)$$

$$\left|\frac{V_{CD}}{V_{AB}}\right| = \frac{\frac{8}{\pi^2}}{\sqrt{1 + \left(\frac{\omega_{Lr} - \frac{1}{\omega_{Cr}}}{\omega_{Lm}}\right)^2 + \left(\frac{\omega_{Lr} - \frac{1}{\omega_{Cr}}}{R_{ac}}\right)^2}} \quad (9)$$

$$\left|\frac{V_{CD}}{V_{AB}}\right| = \frac{\frac{8}{\pi^2}}{\sqrt{\left(1 + \frac{L_r}{L_m} - \frac{L_r}{\omega^2 C_r L_r L_m}\right)^2 + \left(\frac{\omega_{Lr}}{R_{ac}} - \frac{1}{\omega C_r R_{ac}}\right)^2}} \quad (10)$$

From Equation (10), the following can be defined.

- Quality factor: $Q = \frac{\omega_0 L_r}{R_{ac}} = \frac{1}{\omega_0 L_r R_{ac}}$
- Resonant angular frequency: $\omega_0 = \frac{1}{\sqrt{L_r C_r}}$
- Normalized angular frequency: $\omega_x = \frac{\omega}{\omega_0}$
- Normalized frequency: $f_n = \frac{\omega_x}{2\pi}$

Subsequently, the total voltage ratio (M_g) of the input and output including the secondary rectifier diode can be expressed as Equations (11) and (12).

$$M_g = \left|\frac{V_{CD}}{V_{AB}}\right| = \frac{\frac{8}{\pi^2}}{\sqrt{\left(1 + \frac{L_r}{L_m} \left(1 - \frac{1}{\omega_x^2}\right)\right)^2 + Q^2 \left(\omega_x - \frac{1}{\omega_x}\right)^2}} \quad (11)$$

where

$$m = \frac{L_m + L_r}{L_r} \rightarrow \frac{L_m}{L_r} = m - 1$$

$$M_g = \left|\frac{V_{CD}}{V_{AB}}\right| = \frac{\frac{8}{\pi^2} \omega_x^2}{\sqrt{\left(\omega_x^2 + \frac{L_r}{L_m} (\omega_x^2 - 1)\right)^2 + Q^2 \omega_x^2 (\omega_x^2 - 1)^2}} \quad (12)$$

The final M_g can be expressed as follows:

$$M_g = \left|\frac{V_{CD}}{V_{AB}}\right| = \frac{8}{\pi^2} \frac{\omega_x^2 (m - 1)}{\sqrt{(m \omega_x^2 - 1)^2 + Q^2 \omega_x^2 (\omega_x^2 - 1)^2 (m - 1)^2}} \quad (13)$$

4. Analysis of Resonance Characteristics of LLC Resonant Converter

Figure 9 shows the voltage gain curve of the LLC resonant converter versus the frequency.

This figure shows the M_g value when the normalized frequency $\left(\frac{M_g}{2\pi}\right)$ is between 0.3 and 2.5. As shown in Figure 9, for an LLC resonant converter, the reference frequency to be controlled can be defined in different ways considering the resonance characteristics. Generally, when the f_s of the main switch in an LLC resonant converter operates below the f_0 .

When an LLC resonant converter operates in the ZCS region and operates above f_0 , the switching operation is performed in the ZVS region [6,22].

As described above, if the LLC resonant converter is designed under the condition of $f_s = f_0$ or $f_s < f_0$, the efficiency under full and heavy load conditions is excellent, but it is not suitable for lithium-ion battery chargers because the efficiency under light load conditions rapidly decreases [10].

In a rapid charger for battery charging, operating f_s under the condition $f_s > f_0$ is desirable, as it yields excellent efficiency in the entire load range and greatly reduces the circulating current of the resonant circuit [22].

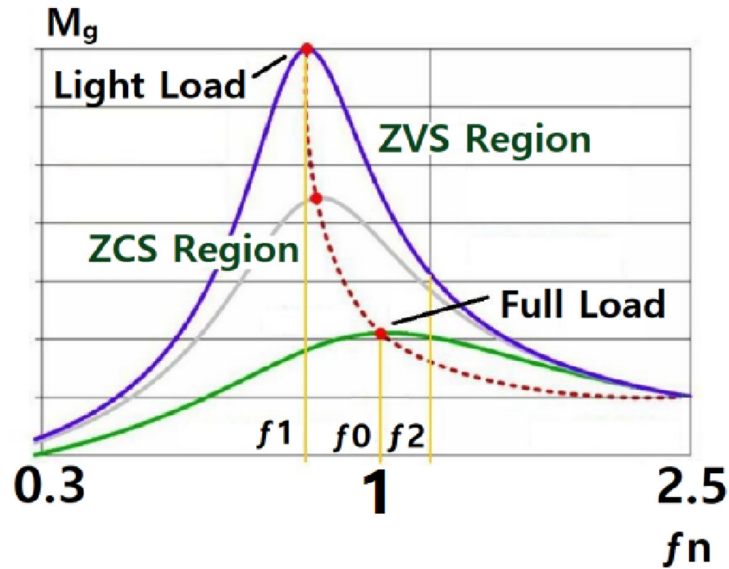


Figure 9. Gain curve of LLC resonant converter according to frequency.

In this study, considering the $m = 1.5, 6.0, 15, 30$ and $Q = 0.1, 0.5, 0.7, 1.0, 5.0, 10.0$ conditions for the proposed LLC resonant AHB converter and the input and output according to the frequency at each load, M_g was simulated using MATLAB Version 9.4.

Figure 10 shows the MATLAB simulation results.

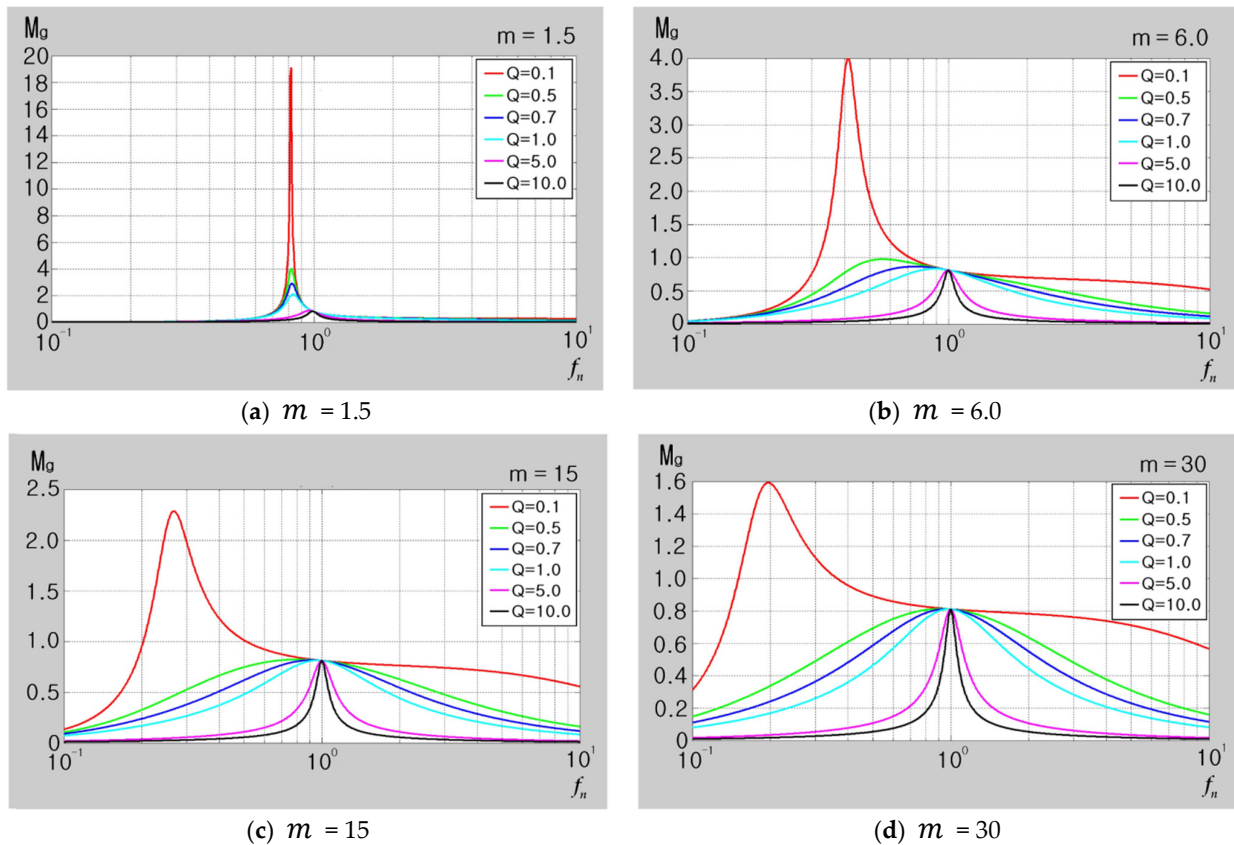


Figure 10. Gain curve of the LLC resonant converter according to frequency using MATLAB.

In Figure 10, the M_g values obtained under the full and light load conditions in the LLC resonant converter are compared.

As seen in Figure 10, when the m value is designed to be small, the change in total voltage gain (M_g) is large between light load and full load. And when the m value is designed to be large, the change in total voltage gain (M_g) is small.

In addition, as the Q value decreases, the load increases and the total voltage gain (M_g) increases, and as the Q value increases, the load decreases and the total voltage gain (M_g) decreases.

5. Smart Battery Charging System

Figure 11 shows the smart battery charging system located at the output stage of the LLC AHB converter.

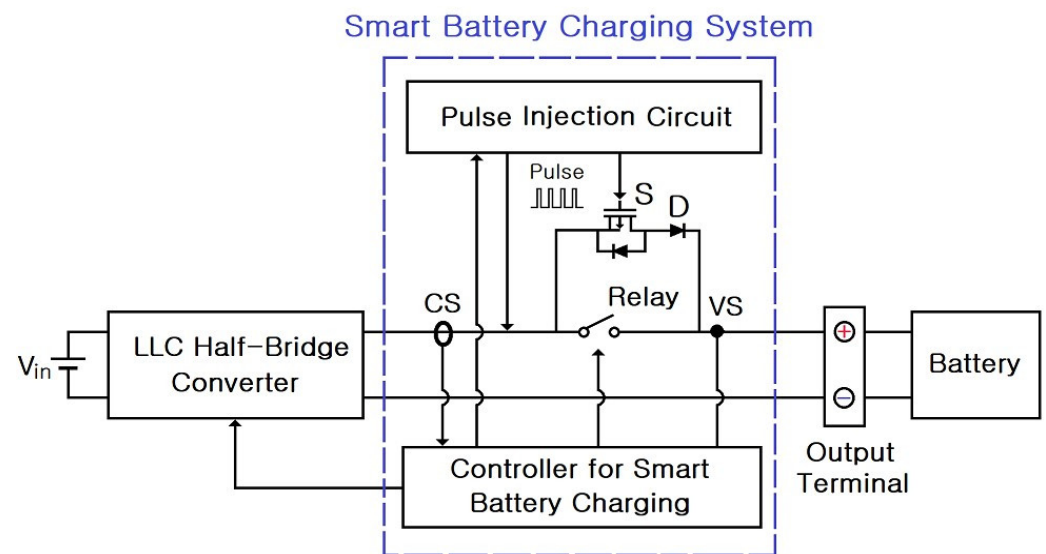


Figure 11. Smart battery charging system placed at the output stage of the LLC half-bridge converter.

The smart battery charging system detects the battery connection through the following process:

- (1) Detect the (+) voltage of the battery through the voltage sensor (VS).
- (2) Inject a 15 V, 0.1 Hz pulse into the (+) terminal of the battery.
- (3) Compare whether the maximum voltage of the pulse is greater than or equal to the minimum voltage of the battery.
- (4) Check whether the current flowing through the battery is 0.5 A through the switch (S) and diode (D).
- (5) Check whether the output voltage of the LLC half-bridge converter and the voltage of the battery are equal.
- (6) Check whether the output voltage of the LLC half-bridge converter and the voltage of the battery are the same.
- (7) The output current of the LLC half-bridge converter gradually increases, and after the maximum output current is reached, the output current gradually decreases.

Figure 12 displays the detailed circuit diagram of the pulse injection circuit of the proposed smart battery charging system. Pulses are continuously injected through the first pulse driving circuit.

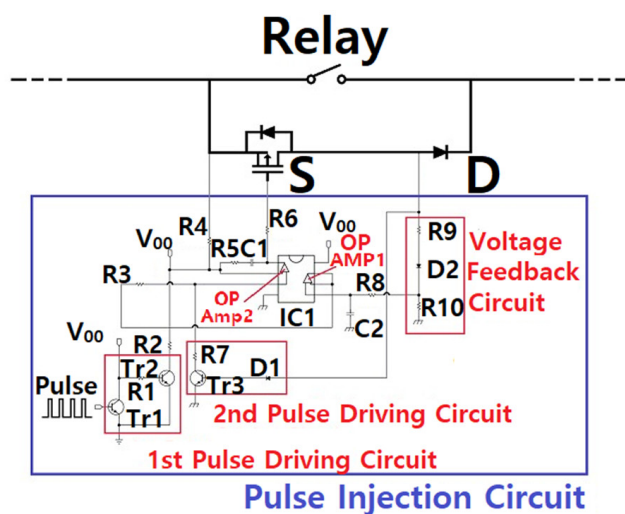


Figure 12. Detailed configuration of the pulse injection circuit.

The voltage feedback circuit detects the battery voltage, and when the maximum value of the pulse voltage matches the battery voltage, the diode (D) conducts. Moreover, the second pulse driving circuit is operated by the first comparator (OP Amp1), and the switch (S) is conducted through the operation of the second comparator (OP Amp2). When the output current detects 0.5 A, the LLC half-bridge converter smartly detects whether the battery is connected to the output terminal and whether the battery voltage is normally generated.

Figure 13 displays the operating waveform of the proposed smart battery charging system. The 15 V, 0.1 Hz pulse train checks whether the battery is properly connected to the output terminal. When the maximum value of the pulse voltage matches the battery voltage, an output current of 0.5 A flows while the diode (D) and switch (S) operate. Thereafter, the output voltage of the LLC half-bridge converter gradually increases, and when the output voltage becomes equal to the battery voltage, the relay is turned on.

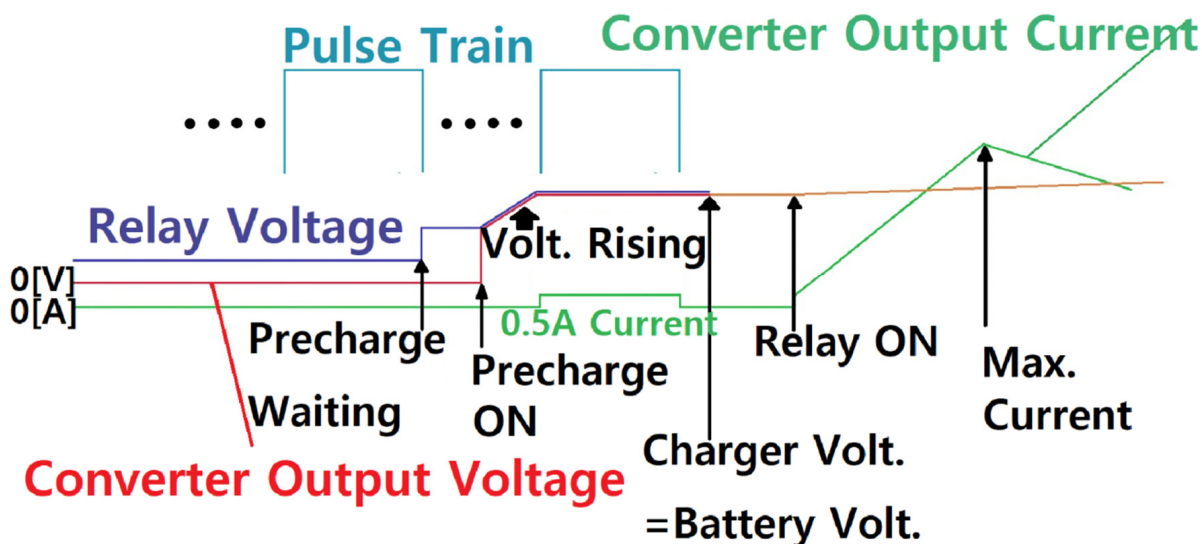


Figure 13. Operating waveform of the smart battery charging system.

Figure 14 shows the battery charging voltage and current waveforms when no smart battery charging system is employed.

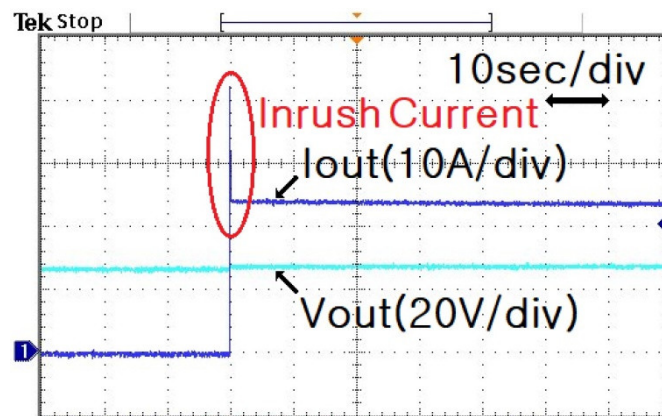


Figure 14. Battery charging voltage and current waveforms without the smart battery charging system.

When the output voltage of the LLC half-bridge converter and the battery voltage differ, a sudden inrush current of more than 40 A is generated in the battery, which impacts the separator of the lithium-ion battery.

Figure 15 shows the battery charging voltage and current waveforms when a smart battery charging system is employed.

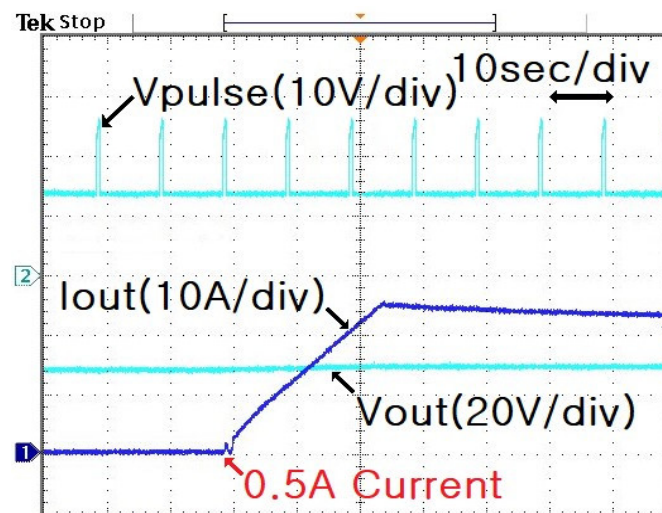


Figure 15. Battery charging voltage and current waveforms with the smart battery charging system.

The proposed charging system detects the normal connection of the battery, gradually matches the output voltage of the LLC half-bridge converter with the battery voltage, and gradually increases the charging current of the lithium-ion battery by gradually increasing the output current of the battery.

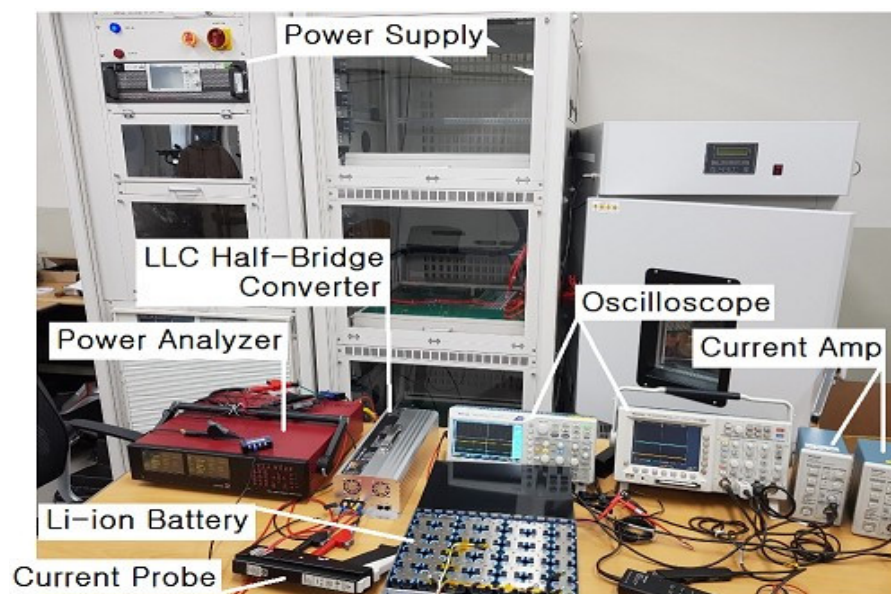
Furthermore, the proposed charging system compares whether the maximum voltage of the pulse train is higher than the battery voltage when the polarity of the battery is reversed, and the relay does not operate when it is high. Thus, the proposed system is effective during mis-wiring and ensures the stable charging of the battery.

6. Simulation and Experimental Results

Table 1 presents the apparatus and circuit parameters used to manufacture the hardware for the personal mobility device rapid charging apparatus. Figure 16 shows the experimental apparatus for the experiment of the proposed circuit and a picture of the manufactured LLC resonant AHB converter, and Figure 17 depicts the simulation circuit of the LLC resonant AHB converter for the proposed fast charging apparatus.

Table 1. Component and circuit parameters used in hardware fabrication.

| | |
|--------------------------------|--|
| Input Voltage (V_{in}) | 100–240 V |
| Output Voltage (V_{out}) | 28 V |
| Output Power (P_{out}) | 1.5 kW (28 V, 50 A) |
| Main Transformer (Trans.) | EE 5040 \times 4, Magnetics N1:N2 = 22:4, Lr = 11.72 μ H |
| Input Capacitor (C_{in}) | 68 μ F \times 6 = 408 μ F |
| Resonant Capacitor (C_r) | 1 μ F |
| Main Switch (S_1, S_2) | OSG60R092H Oriental Semiconductor |
| Secondary Rectifier Diode | NCEP026N10 NCE POWER |
| Output Capacitor (C_{out}) | 1200 μ F \times 8 = 8400 μ F |
| Li-ion Battery | 28 V, 57 Ah, 1500 Wh, Samsung SDI |
| Switching Frequency | 150 kHz |

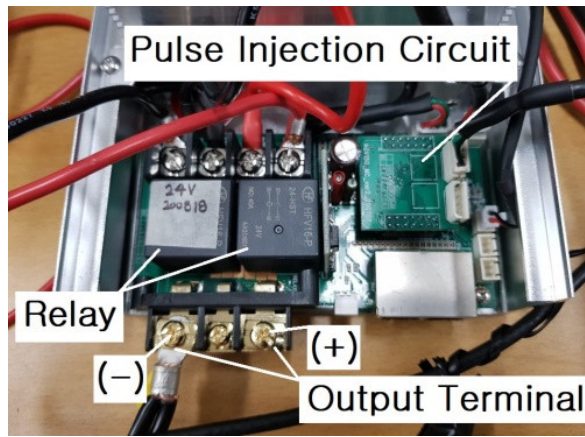


(a)



(b)

Figure 16. Cont.



(c)

Figure 16. Experimental apparatus for the proposed LLC resonant half-bridge converter. (a) Experimental apparatus. (b) Proposed LLC resonant half-bridge converter. (c) Proposed smart battery charging system.

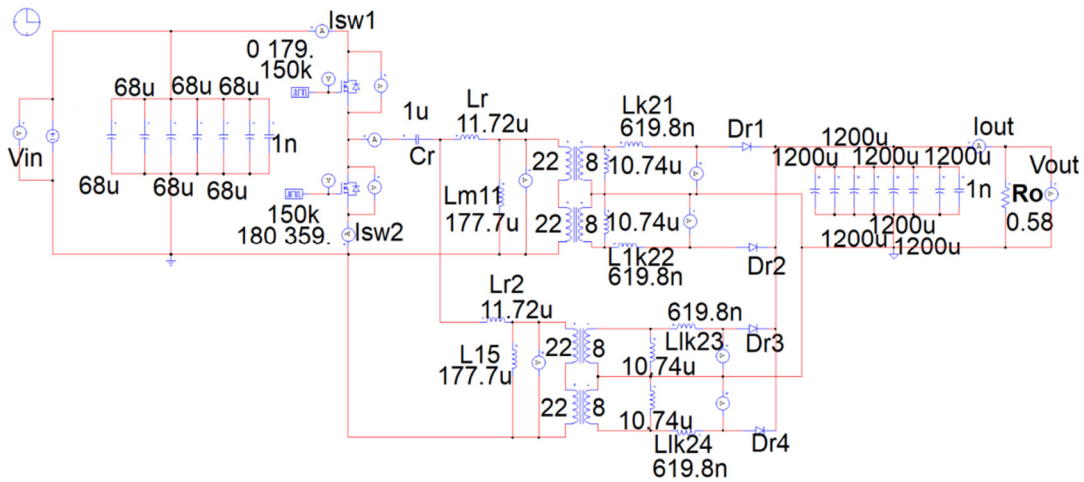


Figure 17. LLC resonant half-bridge converter simulation circuit for the proposed fast charging apparatus (PSIM simulation).

Figure 18 presents the voltage and current simulation waveforms of the upper and lower main switches (S_1 and S_2 , respectively).

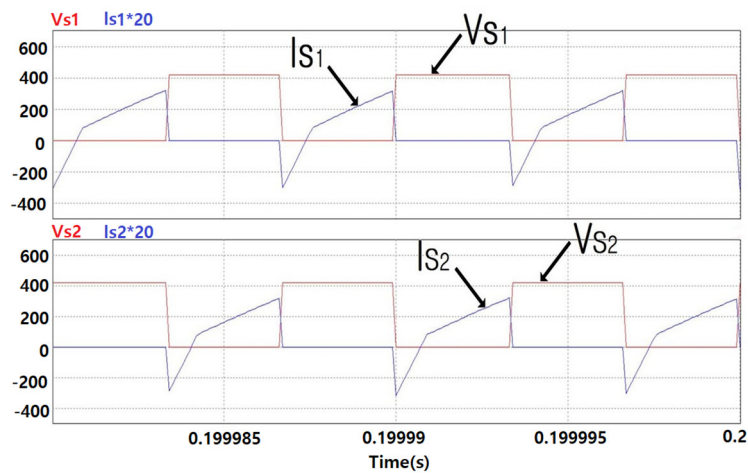


Figure 18. Voltage and current waveforms of the upper and lower main switches (PSIM simulation).

Figure 18 shows that both S_1 and S_2 operate stably with ZVS.

Figures 19 and 20 show the PSIM simulated and experimental waveforms of the gate signal (V_{gate}), low-side switch voltage (V_{S2}), and transformer current (I_{trans}).

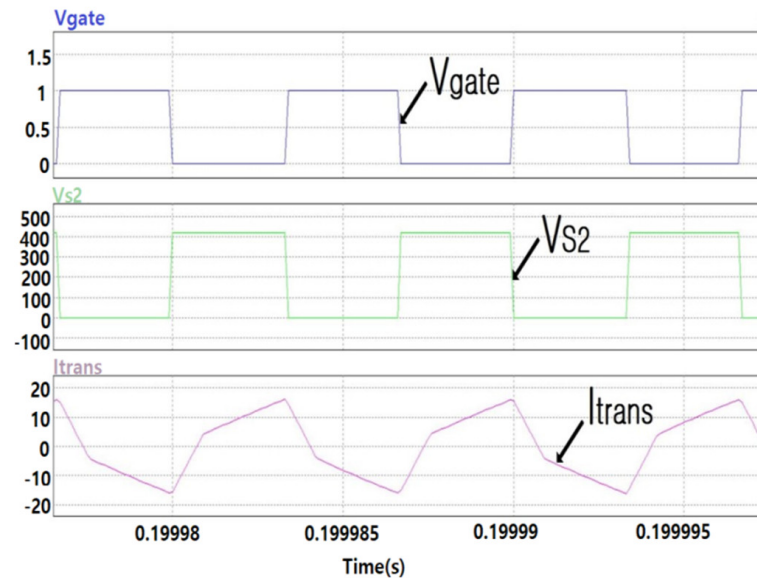


Figure 19. Gate signal, lower switch voltage, and transformer current waveform (PSIM simulation).

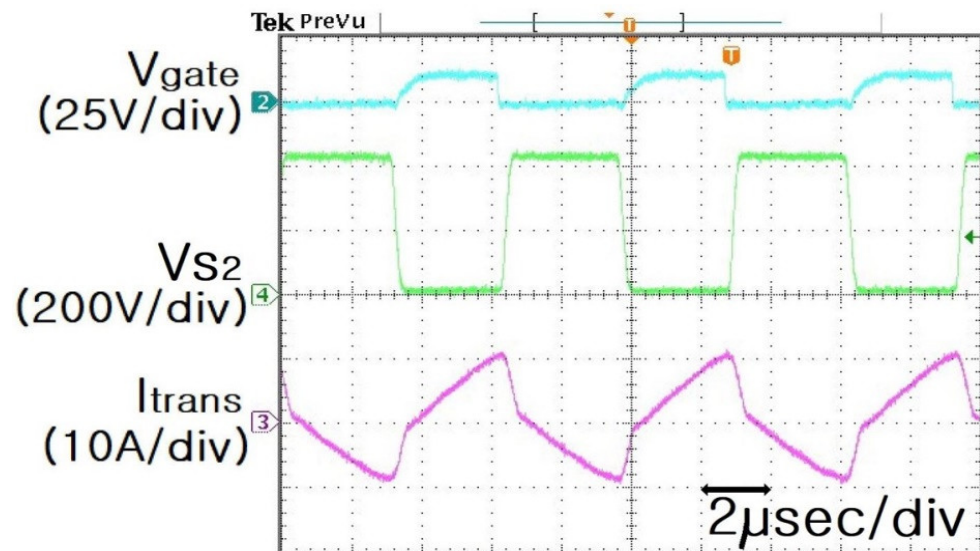


Figure 20. Gate signal, lower switch voltage, and transformer current waveform (experimental waveform).

Comparing the voltage and current waveforms in Figures 19 and 20, the shapes of the waveforms generally match. Thus, the simulations and experiments confirm that f_S operates under the condition of $f_S > f_0$.

Furthermore, the ZVS operation is stably performed without a voltage spike during operation of S_1 and S_2 .

Figure 21 displays the simulation circuit of the LLC resonant half-bridge converter for feedback simulation using PSIM simulation, and Figure 22 exhibits the PSIM simulation waveforms of the load variable output voltage and output current.

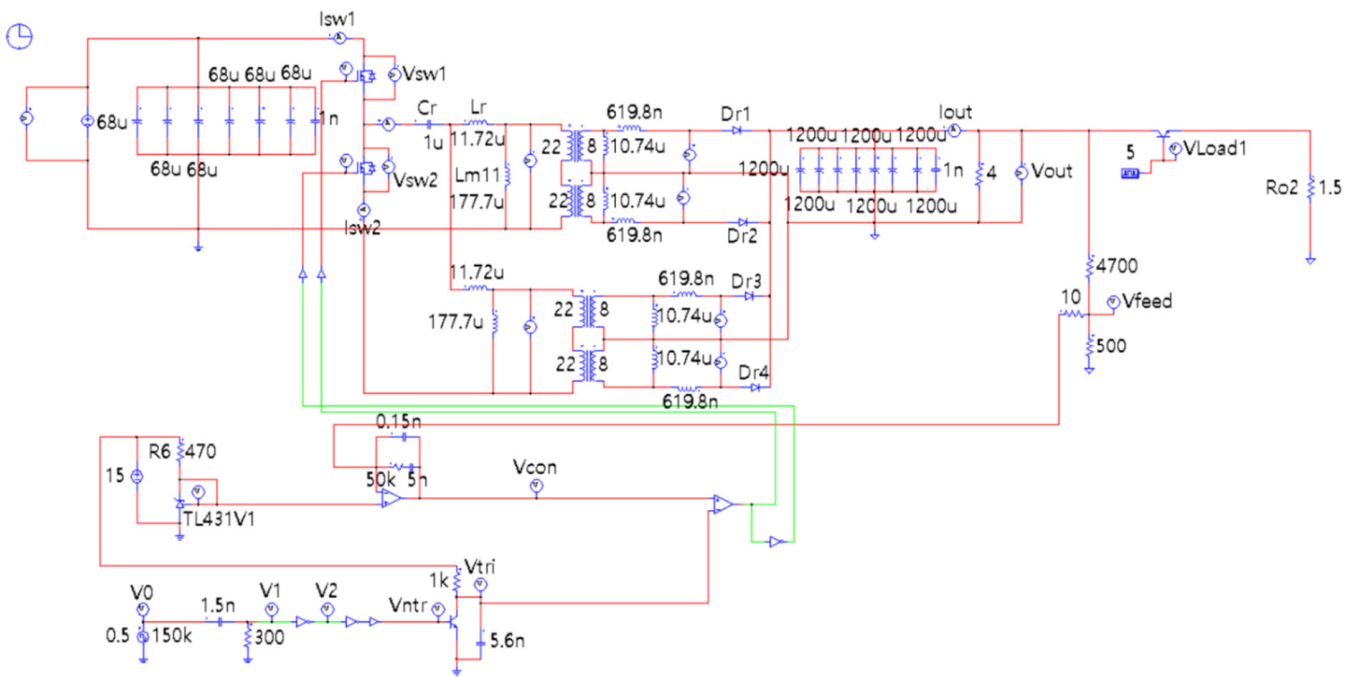


Figure 21. LLC resonant half-bridge converter simulation schematic for load variable feedback simulation (PSIM simulation).

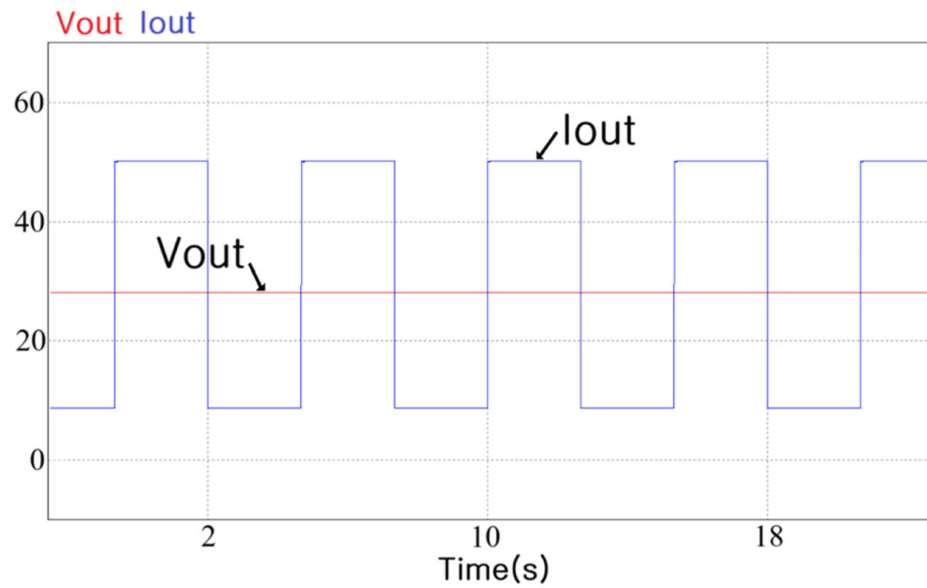


Figure 22. Output voltage and current waveform when load is changed (PSIM simulation).

Figure 23 shows the experimental waveforms of the output voltage and output current obtained when the load is changed.

A comparison of the PSIM simulation waveform in Figure 22 with the experimental waveform in Figure 23 shows that they are almost identical. In Figure 23, the output voltage of the LLC resonant half-bridge converter is tested at 28 V and the load current is varied from 15 to 50 A, which experimentally confirms the stable operation of the LLC resonant half-bridge converter with load changes.

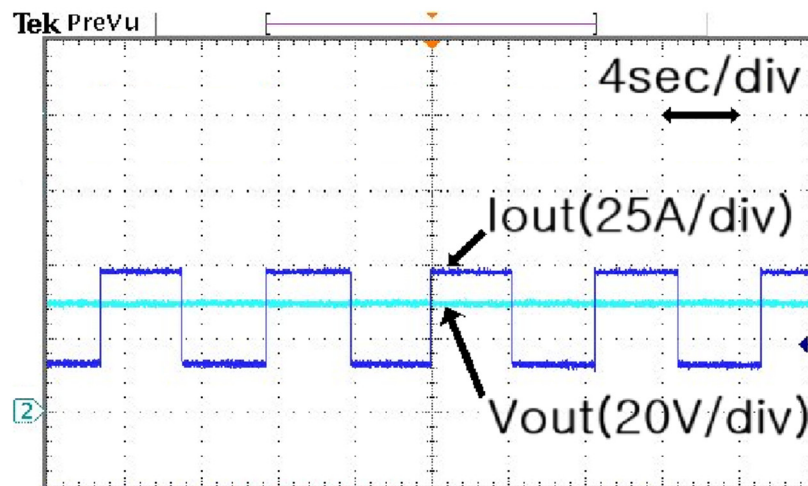


Figure 23. Output voltage and output current waveform when load is changed (experimental waveform).

For the proposed LLC resonant half-bridge converter for the batteries of personal mobility devices, since a large current of 50 A is output at the maximum output current, no inrush current should be generated during initial startup.

Therefore, in the LLC resonant half-bridge converter, the current needs to be gradually increased through the frequency duty control of the main switch.

When an inrush current is generated during the initial start-up, continuous stress is applied to the lithium-ion battery, which may damage the separator of the lithium-ion battery. Subsequently, the lifespan of the battery could be reduced.

Therefore, rapid chargers based on the proposed LLC resonant half-bridge converter are characterized by a gradual increase in the current with a constant slope during the initial startup without the generation of an inrush current.

Figure 24 shows the experimental waveforms of the input voltage, input current, output voltage, and output current at full load.

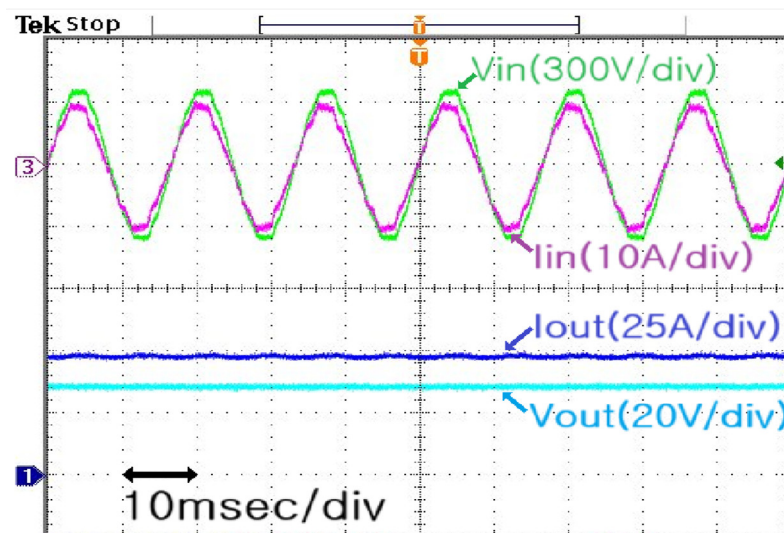


Figure 24. Input voltage, input current, output voltage, and output current waveform at full load (experimental waveform).

Figure 25 presents the efficiency characteristics according to the input voltage and load current. A charging test is performed for a lithium-ion battery using the rapid charger based on the proposed LLC resonant half-bridge converter.

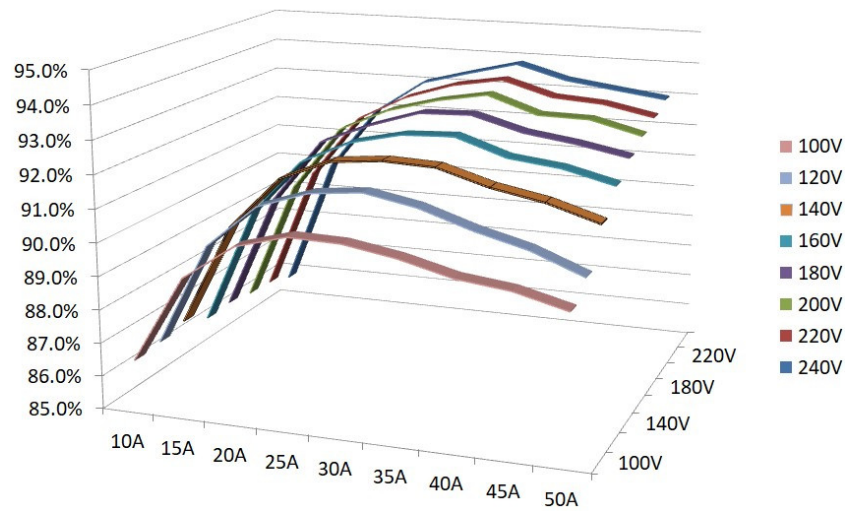


Figure 25. Efficiency characteristics according to input voltage and load current.

The results show that the overall efficiency of the battery is about 86–93%.

The input voltage is varied from 100 to 240 V, and the overall efficiency is measured at the output current of up to 50 A. The efficiency increased with the input voltage and load current.

This experiment verifies that the maximum efficiency is 93.564%, and 28 V, 50 A is stably output without an initial inrush current.

Therefore, the simulations and experiments confirm that the rapid charging apparatus based on the proposed LLC resonant half-bridge converter is suitable for charging the batteries of personal mobility devices.

Table 2 compares the proposed charging system to the previous one.

Table 2. Comparison of Previous and Proposed Charging System.

| Division | Previous Converter without Smart Battery Charging System | Proposed Converter with Smart Battery Charging System |
|----------------------------|---|---|
| Inrush Current | Existing (Max: 20 A) | Does not exist |
| Battery Attached Detection | Output generation regardless of battery attachment | Output is generated only when the battery is attached |
| Additional Effect | <ul style="list-style-type: none"> - Undervoltage Problem - Wrong Wiring Problem - Mis-wiring Problem - Short Circuit Problem | <ul style="list-style-type: none"> - UVP (Undervoltage Protection) - Wrong Wiring Protection - Mis-wiring Protection - Short Circuit Protection |

7. Conclusions

This study proposed an LLC resonant half-bridge converter for the rapid chargers of personal mobility devices.

The operation of each mode of the LLC resonant half-bridge converter were analyzed: $f_s = f_0$, $f_s < f_0$, and $f_s > f_0$.

The LLC resonant AHB converter was used in the charging apparatus of personal mobility devices. In terms of battery charging, a full load or heavy load was initially applied and a light load was continuously applied toward the end. The LLC resonant AHB converter method that operates at $f_s > f_0$, was found to be the most appropriate.

Subsequently, the mathematical modeling of the M_g of the LLC resonant converter operating under $f_s > f_0$ conditions was performed.

The conversion ratio curves of the proposed LLC resonant converter at full and light loads were simulated using the MATLAB program.

Additionally, to validate the proposed method, PSIM was used to simulate and experiment with an LLC resonant AHB converter capable of rapidly charging a 1.5 kW battery.

The proposed charging system detects the normal connection of the battery in real time, starts charging, gradually matches the output voltage of the LLC AHB converter with the battery voltage, and gradually increases the output current of the battery. It smoothly charges Li-ion batteries. If the polarity of the battery is incorrectly connected, the output relay does not operate, thereby improving safety during battery charging. The efficiency of the proposed converter was determined by varying the output voltage of 28 V and the load current from 15 to 50 A. The converter responded stably to the load changes in the experiment, and the maximum efficiency was 93.564%.

The proposed converter is suitable for the rapid charging of micro-electric vehicles and mobility device batteries, and it is expected to have wide application prospects.

Funding: This research was funded by National Research Foundation of Korea (NRF) and the Ministry of Education (MOE): 2021RIS-002.

Data Availability Statement: Data sharing is not applicable.

Conflicts of Interest: The author declares no conflict of interest.

References

1. Brčić, D.; Slavulj, M.; Šojat, D.; Jurak, J. The Role of Smart Mobility in Smart Cities. In Proceedings of the International Conference on Road and Rail Infrastructure, Zadar, Croatia, 17–19 May 2018. [\[CrossRef\]](#)
2. Savithramma, R.M.; Ashwini, B.P.; Sumathi, R. Smart Mobility Implementation in Smart Cities: A Comprehensive Review on State-of-art Technologies. In Proceedings of the International Conference on Smart Systems and Inventive Technology (ICSSIT), Tirunelveli, India, 20–22 January 2022. [\[CrossRef\]](#)
3. Lee, K.; Ahn, T.; Kim, S.; Ryu, B.; Bong, S. A Study on Comparison of Efficiency Characteristics for Half bridge type DC-DC Converters. In Proceedings of the Korean Institute of Power Electronics, (KIPE), Jeju, Republic of Korea, 22–24 June 2006; pp. 356–359.
4. Yong, B.; Lee, F.C.; Cheng, R.; Zhang, A.J.; Huang, G. LLC Resonant Converter for Front End DC/DC Conversion. In Proceedings of the IEEE Applied Power Electronics Conference and Exposition (APEC), Dallas, TX, USA, 10–14 March 2002. [\[CrossRef\]](#)
5. Lu, B.; Liu, W.; Liang, Y.; Lee, F.C.; Wyk, J.D. Optimal Design Methodology for LLC Resonant Converter. In Proceedings of the IEEE Applied Power Electronics Conference and Exposition (APEC), Dallas, TX, USA, 19–23 March 2006; pp. 533–538. [\[CrossRef\]](#)
6. Choi, H.S. Design Consideration of Half-Bridge LLC Resonant Converter. *J. Power Electron.* **2007**, *7*, 13–20.
7. Beiranvand, R.; Zolghadri, M.R.; Rashidian, B.; Alavi, S.M.H. Optimizing the LLC-LC Resonant Converter Topology for Wide-Output-Voltage and Wide-Output-Load Applications. *IEEE Trans. Power Electron.* **2011**, *26*, 3192–3204. [\[CrossRef\]](#)
8. Gu, Y.; Lu, Z.; Hang, L.; Qian, Z.; Huang, G. Three level LLC series resonant DC/DC converter. *IEEE Trans. Power Electron.* **2005**, *20*, 781–789. [\[CrossRef\]](#)
9. Yang, B.; Chen, R.; Lee, F.C. Integrated Magnetic for LLC Resonant Converter. In Proceedings of the IEEE Applied Power Electronics Conference and Exposition (APEC), Dallas, TX, USA, 10–14 March 2002. [\[CrossRef\]](#)
10. Kim, E.S.; Cheng, B.G.; Kang, S.I.; Cha, I.S.; Kye, M.H. A Novel Topology of Secondary LLC Series Resonant Converter. In Proceedings of the IEEE Applied Power Electronics Conference and Exposition (APEC), Anaheim, CA, USA, 25 February–1 March 2007. [\[CrossRef\]](#)
11. Chen, W.; Rong, P.; Lu, Z. Snubberless Bidirectional DC-DC Converter with New CLLC Resonant Tank Featuring Minimized Switching Loss. *IEEE Trans. Ind. Electron.* **2009**, *57*, 3075–3086. [\[CrossRef\]](#)
12. Cheng, J.H.; Witulski, A.F. LLC Parallel Resonant Converter Design by Scaling the LC Converter. *IEEE Trans. Aerosp. Electron. Syst.* **1998**, *34*, 924–933. [\[CrossRef\]](#)
13. Cheng, J.H.; Witulski, A.F. Analytic Solutions for LLCC Parallel Resonant Converter Simplify Use of Two- and Three-Element Converters. *IEEE Trans. Power Electron.* **1998**, *13*, 235–243. [\[CrossRef\]](#)
14. Feng, W.; Huang, D.; Mattavelli, P.; Fu, D.; Lee, F.C. Digital Implementation of Driving Scheme for Synchronous Rectification in LLC Resonant Converter. In Proceedings of the IEEE Energy Conversion Congress and Exposition, Atlanta, GA, USA, 12–16 September 2010; pp. 256–263. [\[CrossRef\]](#)
15. Lin, B.R.; Huang, C.L.; Tseng, C.H. Analysis and Design of Half-Bridge Converter with Two Current Doubler Rectifiers. In Proceedings of the IEEE Conference on Industrial Electronics and Applications, Singapore, 24–26 May 2006. [\[CrossRef\]](#)
16. Mishima, T.; Mizutani, H.; Nakaoka, M. An LLC Resonant Full-Bridge Inverter-link DC-DC Converter with an Anti-resonant Circuit for Practical Voltage Step-Up/Down Regulation. In Proceedings of the IEEE Energy Conversion Congress and Exposition (ECCE), Raleigh, NC, USA, 15–20 September 2012. [\[CrossRef\]](#)
17. Bhat, A.K.S.; Zheng, L. Analysis and Design of a Three-phase LCC-Type Resonant Converter. *IEEE Trans. Aerosp. Electron. Syst.* **1998**, *34*, 508–519. [\[CrossRef\]](#)

18. Yi, K.H.; Moon, G.W. A Novel Two-Phase Interleaved LLC Series-Resonant Converter Using a Phase of the Resonant Capacitor. *IEEE Trans. Ind. Elec.* **2009**, *56*, 1815–1819. [[CrossRef](#)]
19. Gu, Y.; Hang, L.; Lu, Z.; Qian, Z.; Xu, D. Voltage Doubler Application in Isolated Resonant Converters. In Proceedings of the IEEE Industrial Electronics Society (IECON), Raleigh, NC, USA, 6–10 November 2005. [[CrossRef](#)]
20. Mishima, T.; Nakaoka, M. An asymmetrical ZCS-PWM half-bridge DC-DC converter with active auxiliary edge-resonant snubber. In Proceedings of the IEEE International Conference on Industrial Technology (ICIE), Chengdu, China, 21–24 April 2008; pp. 1184–1188. [[CrossRef](#)]
21. Huang, H. Designing an LLC Resonant Half-Bridge Power Converter 2010 Texas Instruments Power Supply Design Seminar. Available online: <https://www.ti.com/seclit/ml/slup263/slup263.pdf> (accessed on 20 July 2023).
22. Han, S.K.; Moon, G.W.; Youn, M.J. A high efficiency ZVS PWM asymmetrical half bridge converter for plasma display panel sustaining power module. In Proceedings of the IEEE Annual Power Electronics Specialists Conference, Aachen, Germany, 20–25 June 2004; pp. 1184–1188. [[CrossRef](#)]
23. Song, M.S.; Lee, J.B. Pulse-Amplitude-Modulation Full-Bridge Diode-Clamped Multilevel LLC Resonant Converter Using Multi-Neighboring Reference Vector Discontinuous PWM. *Energies* **2022**, *15*, 4045. [[CrossRef](#)]
24. Luo, Z.; Wu, Z.; Quan, X.; Xie, X.; Dou, X.; Hu, Q. Synchronous rectification of LLC resonant converters based on resonant inductor voltage. *Front. Energy Res.* **2023**, *11*, 1199397. [[CrossRef](#)]
25. Ahmed, M.H.; Lee, F.C.; Li, Q. Two-Stage 48V VRM With Intermediate Bus Voltage Optimization for Data Centers. *IEEE J. Emerg. Sel. Top. Power Electron.* **2021**, *9*, 702–715. [[CrossRef](#)]
26. Li, Y.; Wei, M.; Luy, X.; Ni, Z.; Cao, D. Analysis and Design of High-Efficiency Modular Multilevel Resonant DC-DC Converter. *IEEE Open J. Power Electron.* **2022**, *3*, 755–771. [[CrossRef](#)]
27. Abdel-Rahim, O.; Chub, A.; Maheri, H.M.; Blinov, A.; Vinnikov, D. High-Performance Buck-Boost Partial Power Quasi-Z-Source Series Resonance Converter. *IEEE Access* **2022**, *10*, 130177–130189. [[CrossRef](#)]

Disclaimer/Publisher’s Note: The statements, opinions and data contained in all publications are solely those of the individual author(s) and contributor(s) and not of MDPI and/or the editor(s). MDPI and/or the editor(s) disclaim responsibility for any injury to people or property resulting from any ideas, methods, instructions or products referred to in the content.